https://doi.org/10.5194/cp-2024-60
Preprint. Discussion started: 18 September 2024

Climate of the Past Discussions

Environmental controls of rapid terrestrial organic matter mobilization to the western Laptev Sea since the last deglaciation

Tsai-Wen Lin[1,2], Tommaso Tesi[3], Jens Hefter[1], Hendrik Grotheer[1,2,4], Jutta Wollenburg[1], Florian Adolphi[1,2,4], Henning Bauch[1,5], Alessio Nogarotto[3], Juliane Müller[1,2,4], Gesine Mollenhauer[1,2,4]

[1]Alfred Wegener Institute, Helmholtz Centre for Polar and Marine Research, 27570, Bremerhaven, Germany
[2]Department of Geosciences, University Bremen, 28334, Bremen, Germany
[3]Institute of Polar Sciences, National Research Council, 40129, Bologna, Italy
[4]MARUM Centre for Marine Environmental Sciences, University Bremen, 28334, Bremen, Germany
[5]GEOMAR, Helmholtz Centre for Ocean Research, 24148, Kiel, Germany

Correspondence to: Tsai-Wen Lin (tsai-wen.lin@awi.de) and Gesine Mollenhauer (gesine.mollenhauer@awi.de)

Abstract. Arctic permafrost stores vast amounts of terrestrial organic matter (terrOM). Under warming climate conditions, Arctic permafrost thaws, releasing aged carbon and potentially impacting the modern carbon cycle. We investigated the characteristics of terrestrial biomarkers, including *n*-alkanes, fatty acids, and lignin phenols, in marine sediment cores to understand how the sources of terrOM transported to the ocean change in response to varying environmental conditions such as sea-level rise, sea ice coverage, inland climate warming, and freshwater input. We examined two sediment records from the western Laptev Sea (PS51/154 and PS51/159) covering the past 17.8 kyr. Our analyses reveal three periods with high mass accumulation rates (MARs) of terrestrial biomarkers, from 14.1 to 13.2, 11.6 to 10.9, and 10.9 to 9.5 kyr BP. These MAR peaks revealed distinct terrOM sources, likely in response to changes in shelf topography, rates of sea-level rise, and inland warming. By comparing periods of high terrOM MAR in the Laptev Sea with published records from other Arctic marginal seas, we suggest that enhanced coastal erosion driven by rapid sea-level rise during meltwater pulse 1A (mwp-1A) triggered elevated terrOM MAR across the Arctic. Additional terrOM MAR peaks coincided with periods of enhanced inland warming, prolonged ice-free conditions, and freshwater flooding, which varied between regions. Our results highlight regional environmental controls on terrOM sources, which can either facilitate or preclude regional terrOM fluxes in addition to global controls.

Short Summary. In order to understand the mechanisms governing permafrost organic matter re-mobilization, we investigated organic matter composition during past intervals of rapid sea-level rise, of inland warming, and of dense sea-ice cover in the Laptev Sea. We find that sea-level rise resulted in wide-spread erosion and transport of permafrost materials to the ocean, but erosion is mitigated by regional dense sea ice cover. Factors like inland warming or floods increase permafrost mobilization locally.

Keywords. Last deglaciation, *n*-alkanes, fatty acids, lignin phenols, permafrost thawing, organic matter mobilization, organic matter mass accumulation rate, lignin phenol flux

https://doi.org/10.5194/cp-2024-60
Preprint. Discussion started: 18 September 2024

Climate of the Past Discussions
Open Access
EGU

1 Introduction

Circumarctic permafrost plays an important role in the Arctic carbon cycle and is strongly affected by rapid Arctic warming, which is greater than the Northern Hemisphere average (Miller et al., 2010; Rantanen et al., 2022). It is one of the main terrestrial carbon sinks at present (Hugelius et al., 2014; Strauss et al., 2017). However, global warming could lead to permafrost thawing, potentially shifting these areas from a carbon sink to a carbon source (Winterfeld et al., 2018; Lara et al., 2019; Laurent et al., 2023). Permafrost is defined as ground that has remained below 0 °C for at least two consecutive years (Dobinski, 2011). Due to the low ground temperature, organic matter stored in permafrost soils remains protected from degradation and release into the modern carbon cycle (Van Everdingen, 2005; Hugelius et al., 2014; Strauss et al., 2017). When permafrost thaws, the organic matter is transported through fluvial networks and coastal erosion to the ocean, eventually being deposited in marine basins (Schuur et al., 2008; Zhang et al., 2022). During thawing and transport, the previously freeze-locked organic matter can be decomposed by microbes, releasing greenhouse gases such as CO_2 and CH_4.

The extent of organic matter degradation from thawing permafrost varies between sources and transportation trajectories (Strauss et al., 2015; Vonk and Gustafsson, 2013). Permafrost deposits from different depths (and ages) are mobilized via different pathways. Initially, increasing land temperatures and precipitation mobilize surface permafrost by deepening the active layer and expanding wetland areas. In later stages, the development of thermokarst and taliks exposes and mobilizes deeper permafrost layers (Schuur et al., 2008). Accelerated coastal erosion facilitates the transport of deep permafrost from cliffs to the ocean, particularly in regions with high cliffs such as the Siberian coast (Vonk and Gustafsson, 2013) (Fig 1). However, permafrost mobilization caused by accelerated coastal erosion can be mitigated by the presence of land-fast sea ice (Rachold et al., 2000; Overduin et al., 2016; Irrgang et al., 2022; Nielsen et al., 2020). Understanding the dominant pathways of permafrost mobilization under different environmental conditions is critical for evaluating the response of Arctic permafrost to future warming. Changes in terrestrial organic matter (terrOM) mobilization and environmental conditions can be recorded in marine sedimentary archives.

Paleoclimate records from the last deglaciation to the early Holocene (c.a., between 19 and 11 kyr BP) offer insights into Arctic permafrost changes in response to warming and rising sea levels (Clark et al., 2012). During the last deglaciation, atmospheric CO_2 concentrations increased, and global sea levels rose, including rapid events and meltwater pulses (Lambeck et al., 2014; Köhler et al., 2017). Rapid increases in atmospheric CO_2 concentration occurred at 16.4, 14.6, and 11.5 kyr BP. The 14.6 kyr BP event coincided with an accelerated global sea-level rise and a period of reduced Arctic sea ice cover, while the 11.5 kyr BP event coincided with intensified inland warming and a drop in sea ice cover in the Arctic (Marcott et al., 2014; Lambeck et al., 2014; Brosius et al., 2021; Detlef et al., 2023; Fahl and Stein, 2012; Müller and Stein, 2014). Studying these periods of rapid environmental change can improve the understanding of how current abrupt warming, sea ice loss, and sea-level rise might affect permafrost stability and the release of previously freeze-locked carbon.

Marine sedimentary archives from the Laptev Sea covering the early period of the last deglaciation (>14 ka BP) are scarce, and existing records often have low temporal resolution and are discontinuous (Martens et al., 2020; Tesi et al., 2016a; Keskitalo et al., 2017; Martens et al., 2019). Here, we present two high-resolution sediment core records that have continuously covered the last 17.8 kyr. We characterize the properties of organic matter exported from Siberian permafrost and relate changes in terrestrial carbon sources to respective climatic conditions. Further, we explore the interplay of potential factors driving rapid terrestrial carbon translocation, including sea-level fluctuations, inland permafrost stability, and variations in sea-ice cover.

https://doi.org/10.5194/cp-2024-60
Preprint. Discussion started: 18 September 2024

Climate of the Past Discussions
Open Access
EGU

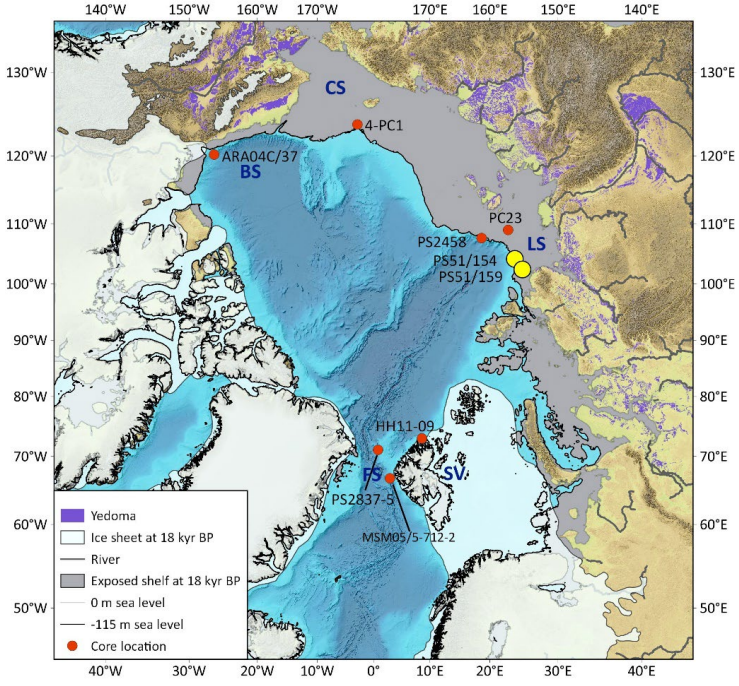

Fig 1. Map of the Arctic Ocean. The names of the marginal seas and archipelago are indicated by acronyms (BS: Beaufort Sea, CS: Chukchi Sea, LS: Laptev Sea, SV: Svalbard archipelago, FS: Fram Strait). The purple area indicates the modern Yedoma domain (Strauss et al., 2021; Strauss et al., 2022; Strauss et al., 2016). The white area shows the ice sheet cover at 18 ka BP (Hughes et al., 2016; Dyke et al., 2003). Grey lines indicate the main river streams in the Arctic (Lehner and Grill, 2013). The exposed continental shelf area at 18 kyr BP is labeled in grey. The black line is the −115 m contour line, which is approximately the sea level at the early period of the last deglaciation (18 kyr BP) (Klemann et al., 2015). Yellow dots show the cores from the Arctic used in this study, including PS51/154 and PS51/159. Red dots show the other cores from previous studies that are used for comparison, including cores ARA04C/37 (Wu et al., 2020), 4-PC1 (Martens et al., 2019), PC23 (Tesi et al., 2016b), PS2458 (Spielhagen et al., 2005), HH11-09 (Nogarotto et al., 2023), PS2837-5 (Birgel and Hass, 2004), and MSM05/5-712-2 (Müller and Stein, 2014; Aagaard-Sørensen et al., 2014; Zamelczyk et al., 2014). The map background is from the International Bathymetric Chart of the Arctic Ocean (IBCAO) (Jakobsson et al., 2012).

2 Study area

The Laptev Sea is a marginal sea of the Arctic Ocean located north of Siberia (Fig 1). The average depth of the Laptev Sea shelf is around 50 m, with a sharp shelf break located between 70 and 100 m water depth. Several sediment-filled paleo river channels cut through the shelf (Kleiber and Niessen, 2000). Due to its shallow water depth and flat topography, the Laptev Sea shelf is highly sensitive to sea-level fluctuations. During the last glacial maximum, the Laptev Sea shelf was not covered by an ice sheet and was exposed during the low sea level stand (Hughes et al., 2016), allowing the accumulation of permafrost deposits. The majority of the shelf was inundated between 12 and 6.5 kyr BP, with the rate of inundation slowing down thereafter (Klemann et al., 2015; Jakobsson et al., 2012) (Fig 2g). This rapid shelf inundation led to southward shifts in both the coastline and the locations of major sediment deposition, causing a significant reduction in sediment input to the outer shelf (Bauch et al., 1999; Mueller-Lupp et al., 2000; Bauch et al., 2001). Today, in the Laptev Sea, sediments from water depths < 10 m are transported further offshore, and the primary deposition center is located at around 30 m water depth (Kuptsov and

https://doi.org/10.5194/cp-2024-60
Preprint. Discussion started: 18 September 2024

Climate of the Past Discussions

Lisitsin, 1996; Are et al., 2002). The Laptev Sea plays a crucial role in the Arctic climate through extensive heat exchange with the atmosphere in summer and sea ice formation in winter, making it a key region for studying the boundary conditions of the Arctic environment's response to climate change (Liu et al., 2022; Rudenko et al., 2014). The Laptev Sea shelf receives substantial sediment inputs from both coastal erosion and river discharge (Mcclelland et al., 2016; Lantuit et al., 2011). Due to high cliffs and intensified wave-induced erosion resulting from summer sea ice melt, the Laptev Sea receives a large proportion of terrestrial material from coastal erosion. Erosion rates along the Laptev Sea coast are higher (0.7 m yr^{-1}) compared to the Arctic coastal average (0.5 m yr^{-1}) and may even reach more than 10 m yr^{-1} (Lantuit et al., 2011; Rachold et al., 2000; Günther et al., 2015). Additionally, the Lena River serves as the primary source of riverine sediments (Holmes et al., 2021; Mcclelland et al., 2016), but coastal erosion contributes more than twice the amount of terrestrial export compared to riverine sources (Rachold et al., 2000).

Most of the water discharged by the Lena River is transported eastward and northward, driven by local winds, carrying suspended sediments in the same direction, and guided by the sea bottom relief (Dmitrenko et al., 1999; Guay et al., 2001). In summer, drift ice and river discharges trigger high productivity of the Laptev Sea shelf (Hörner et al., 2016; Ovsepyan et al., 2015). Large amounts of terrigenous suspended particles in the Laptev Sea are incorporated into the sea ice (Dethleff, 2005). This terrigenous-material-rich sea ice is transported to the Fram Strait by the Transpolar Drift, accounting for 20 % of the total sea ice flow to the Fram Strait (Stein and Macdonald, 2004; Rigor and Colony, 1997).

3 Materials and methods

3.1 Materials

Marine sediment cores PS51/154-11 (77.276 °N, 120.610 °E, water depth 270 m, abbreviated as PS51/154) and PS51/159-10 (76.768 °N, 116.032 °E, water depth 60 m, abbreviated as PS51/159) were obtained with Kasten corers during the ARK-XIV/1b (PS51 Transdrift-V) expedition in August 1998 aboard the R/V *Polarstern* (Kassens, 2016). Core PS51/154 was taken from the upper continental slope, and core PS51/159 from the outer continental shelf (Fig 1). After retrieval, the sediment cores were stored at −20 °C and subsampled at 4 °C. Subsamples were collected with 10 mL syringes from the cores in 5–10 cm intervals. The sampling intervals in core PS51/154 corresponded to an average temporal resolution of approximately 120 yr before 10 kyr BP, and for core PS51/159, the average temporal resolution was about 270 yr. Due to the spatial proximity and consistency of biomarker proxy records between the two cores, we used the PS51/159 record to complement the low temporal resolution in core PS51/154 during the Holocene.

3.2 Microfossil radiocarbon dating and age-depth model

The age-depth models for cores PS51/154 and PS51/159 are based on microfossil ^{14}C ages, initially established by Bauch et al. (2001), modified by Taldenkova et al. (2010) and Hörner et al. (2016), and refined in this study. Six new microfossil radiocarbon dates from core PS51/154 and one from core PS51/159 were added to the existing data sets (Table 1). Sediments were wet-sieved through a 63 µm mesh, and bivalve shell fragments were picked from the > 63 µm and oven-dried sediment fraction. Bivalve shells were examined under a microscope for species identification and photographic records (Table 1). Samples containing more than 250 µgC were converted to graphite targets, while samples containing less than that were analysed as CO_2 gas using the gas interface system

https://doi.org/10.5194/cp-2024-60
Preprint. Discussion started: 18 September 2024

Climate of the Past Discussions
Open Access
EGU

(Table 1). Both types of analysis were conducted using the MIni CArbon Dating System (MICADAS) accelerator mass spectrometer at AWI (Mollenhauer et al., 2021). We used the Marine20 curve for calibration (Heaton et al., 2020), with a time constant ΔR = −95 ± 61 yrs determined from bivalves in the Laptev Sea (Bauch et al., 2001). The dating results are reported as calibrated ages (cal. yr BP). Age-depth models were constructed using OxCal
145 software 4.4 (Bronk Ramsey, 2009), with low model agreement datapoints identified as outliers and removed from the age-depth model. The outlier data are still shown in Table 1 and Fig S1.

Table 1. Radiocarbon dates of cores PS51/154 and PS51/159. The calibrated ages are shown as median ages, with 94.5 % probability ranges in brackets. The ages were calibrated against Marine20 curve (Heaton et al., 2020), with ΔR = −95 ± 61 yrs.

Lab ID	Depth (cm)	Material	Radiocarbon age (yrBP)	Calibrated age (cal.BP)	Reference
PS51/154-11					
KIA-27682	25	foraminifers/ *Yoldiella sp.*	3425±30*	3302 (3529−3044)	Taldenkova et al. (2010)
KIA-6919	31	*Yoldiella intermedia*	1540±45		Bauch et al. (2001)
KIA-32811	39	bivalves/gastropods	1800±35		Taldenkova et al. (2010)
KIA-32810	39	foraminifers	5040±50*	5343 (5570−5065)	Taldenkova et al. (2010)
KIA-27683	51	foraminifers /ostracods/*Yoldiella sp.*	9570±60*	10286(10530−10024)	Taldenkova et al. (2010)
KIA-32812	73	foraminifers	9410±70*	10343(10561−10117)	Taldenkova et al. (2010)
KIA-32813	73	*Yoldiella lenticula*	9605±45		Taldenkova et al. (2010)
KIA-27684	85	foraminifers /*Portlandia arctica*	9505±50*	10389(10604−10151)	Taldenkova et al. (2010)
KIA-32814	115	*Yoldiella lenticula*	9630±50*	10566(10864−10263)	Taldenkova et al. (2010)
KIA-32815	131	*Nucula tenuis*	10085±45*	11156(11348−10857)	Taldenkova et al. (2010)
KIA-6920	138	*Macoma calcarea*	10120±55*	11182(11383−10890)	Bauch et al. (2001)
KIA-6921	204	*Nucula tenuis*	10235±45*	11381(11641−11124)	Bauch et al. (2001)
11524.1.1	223.5	*Macoma calcarea*	10145±104*	11463(11740−11170)	This study[2]
11525.1.1	247	*Macoma calcarea*	10482±91*	11702(12039−11330)	This study[2]
KIA-6922	300	*Yoldiella intermedia*	10725±50*	12183(12475−11834)	Bauch et al. (2001)
	339.5	bivalves	12040±55*	13479(13712−13243)	Hörner et al. (2016)
KIA-6923	375	*Yoldiella lenticula*	12180±60*	13663(13882−13436)	Bauch et al. (2001)
11526.1.1	392.5	*Macoma calcarea*	12257±35*	13741(13963−13514)	This study[1]
11527.1.1	420.5	*Macoma calcarea*	12189±97*	13850(14090−13582)	This study[2]
KIA-6924	440	*Yoldiella intermedia*	12525±55*	14091(14417−13777)	Bauch et al. (2001)
KIA-6925	518	foraminifers /*Portlandia arctica*	13120±60*	15113(15427−14804)	Bauch et al. (2001)
11529.1.1	520.5	*Macoma calcarea*	12855±122		This study[2]
11528.1.1	530.5	*Yoldiella sp.*	14502±44		This study[1]
KIA-9976	567	foraminifers	13540±90*	15659(15971−15339)	Taldenkova et al. (2010)
KIA-9977	569	foraminifers	13570±110*	15687(16006−15365)	Taldenkova et al. (2010)
PS51/159-10					

https://doi.org/10.5194/cp-2024-60
Preprint. Discussion started: 18 September 2024

Climate of the Past Discussions

KIA-6927	11	*Macoma sp.*	845±30*	380547−175)	Bauch et al. (2001)
11523.1.1	32.5	*Portlandia arctica*	2940±24*	2633(2841−2391)	This study[1]
KIA-6928	56	*Portlandia arctica*	4980±35*	5194(5446−4944)	Bauch et al. (2001)
	72.5	bivalve	6610±40		Hörner et al. (2016)
KIA-6929	90	*Portlandia arctica*	6305±35*	6629(6865−6399)	Bauch et al. (2001)
KIA-6930	131	*Portlandia arctica*	8955±40*	9526(9790−9305)	Bauch et al. (2001)
KIA-6931	215	*Portlandia arctica*	9420±50*	10160(10416−9886)	Bauch et al. (2001)
KIA-6932	315	*Portlandia arctica*	9650±45*	10501(10773−10230)	Bauch et al. (2001)
KIA-6933	410	*Portlandia arctica*	10720±55*	12012(12376−11703)	Bauch et al. (2001)
KIA-6934	485	*Portlandia arctica*	11060±70*	12517(12732−12210)	Bauch et al. (2001)

***Dating results that were taken for the age-depth model calculation. [1]Sample analysed as graphite. [2]Sample analysed as CO2 gas.**

3.3 Bulk analysis

Stable carbon isotope compositions of total organic carbon ($\delta^{13}C$) in cores PS51/154 and PS51/159 were analysed using 15 mg of freeze-dried, homogenized sediment acidified with 1.5 M HCl in silver boats to remove carbonate. The acidified samples were then dried in the oven at 55 ˚C. $\delta^{13}C$ values were measured using a Thermo Scientific FLASH 2000 CHNS Analyser coupled with a Thermo DeltaQ IRMS via CONFLO IV at the Institute of Polar Sciences, National Research Council (CNR-ISP). $\delta^{13}C$ values were reported in parts per thousand (per mil, ‰) relative to Vienna Pee Dee Belemnite (VPDB). The standard error for replicate analyses of in-house standards was less than 0.15 ‰.

3.4 Lipid extraction and analysis

The lipid extractions were done following the procedure by Winterfeld et al. (2018). 1–5 g of freeze-dried, homogenized sediment samples were weighed and subsequently submerged in 25 mL dichloromethane (DCM) + methanol (v/v = 9/1) followed by ultrasonication (15 mins) for three times to acquire total lipid extracts (TLE). An internal quantification standard containing 889.6ng squalane and 1558 ng 19-methylarachidic acid were added before extraction. After drying the TLE under a stream of nitrogen, the TLE was saponified using 1 mL of 0.1 M potassium hydroxide (KOH) in methanol/H_2O (v/v = 9:1) at 80 °C for 2 h. After saponification, the neutral lipids (NLs) were extracted from the TLE with 3x1 mL hexane. Hydrochloric acid (HCl, 37 %) was added to acidify the remaining TLE until pH < 2, and the fatty acids (FAs) were subsequently extracted with 3 x 1 mL DCM. The neutral lipids (NLs) were further separated into three polarity fractions of hydrocarbons (containing alkanes), ketones, and polar lipids through a silica column by eluting with 4 mL of hexane, DCM + hexane (v/v = 2:1), and DCM + methanol (v/v = 1:1), respectively. The fatty acids (FAs) were methylated by adding 40 µL 37 % HCl and 1 mL methanol and heated to 50 °C for >12 h to form fatty acid methyl esters (FAMEs). Prior to sealing, the head-space of the sample vials was filled with pure nitrogen gas. The FAME fraction was extracted from the methanol solution with 3 x 1 mL hexane after methylation was completed.

The hydrocarbon and FAME fractions were analysed with an Agilent 7890A gas chromatograph equipped with a flame ionization detector (GC-FID) using an Agilent J&W DB-5MS column (60m × 250 µm × 0.25 µm-thick film). The oven was held at 60 °C for 1min, heating at a ramp of 20 °C min^{-1} to 150 °C and to 320 °C at 6 °C min^{-1}, with

https://doi.org/10.5194/cp-2024-60
Preprint. Discussion started: 18 September 2024

Climate of the Past Discussions
Open Access
EGU

the final holding time of 35 min. $C_{15–34}$ *n*-alkanes and $C_{14–32}$ fatty acids were identified by comparing the retention times of a *n*-$C_{10–40}$ *n*-alkane standard mix and a *n*-$C_{28:0}$ FAME standard, respectively. The uncertainty was calculated as the average of the absolute differences between the mean values from duplicate analyses; this was expressed as standard variation (cf. Grotheer et al., 2015). The uncertainty of the total contents of *n*-alkanes was 11.6 % (*n* = 62), and of FAMEs was 12.8 % (*n* = 68).

3.5 Lignin phenol extraction and analysis

The extraction procedure for lignin-oxidation products was modified from the protocol described by Goñi and Montgomery (2000). About 200–300 mg dried and homogenized samples, around 300 mg Copper oxide (CuO), around 50 mg ferrous ammonium sulfate, and 6 mL NaOH (2 N) were added into a Teflon tube in an oxygen-free environment (O_2 < 1.0 %). Samples were oxidized in a microwave digestion system (MARS 6) at 150 °C for 90 mins. Afterward, 9.75 µg of ethyl vanillin (Evl) was added as an internal standard; the samples were then centrifuged, and the supernatant was recovered. The solutions were acidified with 3 mL HCl (6 N). The CuO oxidation products, including lignin phenols, were recovered by liquid/liquid extraction with 2 x 5 mL ethyl acetate. Sodium sulfate (Na_2SO_4) was added to the ethyl acetate extract to remove any remaining water. The extracts were evaporated to dryness using a rotational vacuum concentrator and were subsequently transferred into analytical vials with 500 µL pyridine for later analysis. Prior to analysis, 40 µL of the extracts dissolved in pyridine were silylated by adding 40 µL N,O-Bis(trimethylsilyl)trifluoroacetamide with 1 % Trimethylchlorosilane and reacted at 50 °C for 15 mins. The CuO oxidation products were analysed with an Agilent Technologies 7820A gas chromatograph coupled with a 5977B MSD mass selective detector (GC-MS) equipped with a 30m × 320 µm × 0.25 µm-thick film column (Trajan SGE PB-1). The oven was set from 95 °C to 300 °C at a heating ramp of 4 °C min^{-1} with a holding time of 10 min. Here we focused on 3,5-dihydroxybenzoic acid (3,5 Bd) and three lignin phenol groups, including (1) Vanillyl phenols (V): including vanillin (Vl), acetovanillone (Vn), and vanillic acid (Vd). (2) Syringyl phenols (S): including syringaldehyde (Sl), acetosyringone (Sn), and syringic acid (Sd). (3) Cinnamyl phenols (C): including p-coumaric acid (p-Cd) and ferulic acid (Fd). The uncertainty of the total content for lignin phenols was 6.9 % (*n* = 10).

3.6 Biomarker parameters

The biomarker parameters we used in this study are listed below. The P_{aq} index was calculated as the content ratio of mid-chain over long-chain (also recognized as high molecular weight, HMW) *n*-alkanes. As aquatic macrophytes are known to synthesize more mid-chain *n*-alkanes and leaf-waxes of terrestrial plants contain more HMW *n*-alkanes, a higher P_{aq} value indicates a higher contribution from aquatic macrophytes and, therefore, is commonly used to trace wetland input in marine sediments (Ficken et al., 2000; Meyer et al., 2019; Alves et al., 2023). The calculation followed Eq. 1 from Ficken et al. (2000). The C_n represents the content of *n*-alkane homologs. The uncertainty of P_{aq} was 0.008 based on the average standard variation of 31 pairs of duplicate analyses (*n* = 62).

$$P_{aq} = \frac{C_{23}+C_{25}}{C_{23}+C_{25}+C_{29}+C_{31}} \quad (1)$$

We used the HMW fatty acids to calculate the temporal change in mass accumulation rate (MAR) to evaluate the terrOM flux into marine basins. Fatty acids in higher plants are dominated by even-numbered HMW saturated

https://doi.org/10.5194/cp-2024-60
Preprint. Discussion started: 18 September 2024

Climate of the Past Discussions
Open Access
EGU

fatty acids (Bianchi and Canuel, 2011). The MAR of HMW fatty acids was calculated from Eq. 2. S represents the sedimentation rate (cm yr^{-1}), ρ refers to dry bulk density (g cm^{-3}), and the $C_{24:0}$, $C_{26:0}$, $C_{28:0}$, $C_{30:0}$ are the contents of the HMW n-fatty acids per gram of dry sediment (mg g^{-1}). The unit of MAR is mg cm^{-2} kyr^{-1} (data in Table S1 and Table S2). The average uncertainty of HMW fatty acids MAR was 14.1 % (n = 68). One can also use other indices that represent the terrOM source. We calculated the MARs of HMW *n*-alkanes and lignin phenols in cores PS51/154 and PS51/159 as well. The patterns between all the MARs were identical (Fig S3). Here, we only show the MAR of HMW fatty acids for a better comparison to previous studies (Winterfeld et al., 2018; Meyer et al., 2019; Alves et al., 2023).

$$\mathrm{MAR} = \mathrm{S} \times \rho \times (C_{24:0} + C_{26:0} + C_{28:0} + C_{30:0}) \quad (2)$$

We used lignin phenols to calculate three indices. The syringic acid over syringaldehyde ratio (Sd/Sl) reflects the degree of degradation of lignin in the sediments, with higher Sd/Sl indicating more degraded lignin (Haddad et al., 1992; Hedges et al., 1988). The uncertainty of Sd/Sl was 0.02 based on the average standard variation of five pairs of duplicate analyses (n = 10). The syringyl phenols over vanillyl phenols ratio (S/V) indicates the relative contribution of gymnosperm and angiosperm sources, and the cinnamyl phenols over vanillyl phenols ratio (C/V) illustrates the relative contribution of woody and non-woody tissue, respectively (Hedges and Mann, 1979; Goñi and Hedges, 1992; Tesi et al., 2010). The combination of S/V and C/V ratios is a good indicator for identifying lignin phenol sources. The S/V ratio and C/V ratio were calculated with the lignin phenol contents, as shown in Eq. 3 and Eq. 4. The uncertainty of S/V was 0.003 (n = 10), and of C/V is 0.01 (n = 10).

$$\frac{\mathrm{S}}{\mathrm{V}} = \frac{Sl+Sn+Sd}{Vl+Vn+Vd} \quad (3)$$

$$\frac{\mathrm{C}}{\mathrm{V}} = \frac{pCd+Fd}{Vl+Vn+Vd} \quad (4)$$

4 Results

4.1 Chronology and organic matter mass accumulation rates in cores PS51/154 and PS51/159

An updated age-depth model for core PS51/154 was established with 15 radiocarbon dates and for core PS51/159 with 11 radiocarbon dates (Table 1, Fig S1, Fig S2). Core PS51/154 covered the period from 17.5 to 3.0 kyr BP. Three periods of peak sedimentation rates were found: during the end of Bølling-Allerød (from 14.1 to 13.2 kyr BP), the Preboreal (from 11.6 to 10.9 kyr BP), and the early Holocene (from 10.9 to 10.1 kyr BP). After 10.1 kyr BP, the sedimentation rate in core PS51/154 dropped drastically. Core PS51/159 covered the period from 11.9 to 0.3 kyr BP, with a peak of sedimentation rate during the early Holocene (from 10.6 to 9.5 kyr BP), followed by a significant sedimentation rate drop afterward. The mass accumulation rates (MARs) of all biomarkers were largely affected by the pronounced sedimentation rate changes and thus, showed similar temporal changes in all terrestrial biomarkers, including HMW *n*-alkanes, HMW fatty acids, and lignin phenols (Fig S3, contents of each biomarker in Fig S4). Fig 2a and Fig 5 i, j show the mass accumulation rate of HMW fatty acids as a representation.

4.2 Bulk organic records in cores PS51/154 and PS51/159

The record before 16.2 kyr BP in core PS51/154 was characterized by high $\delta^{13}C$ (−23.8 ‰) and low TOC values (0.57 %) (Fig S5). A slump layer at 15.4 kyr BP (530–540 cm) was identified by increased grain size (Taldenkova et al., 2010) and a drop in total organic matter (TOC) (Hörner et al., 2016) (Fig S5). However, the $\delta^{13}C$ value did

https://doi.org/10.5194/cp-2024-60
Preprint. Discussion started: 18 September 2024


Climate of the Past Discussions

not show a significant change at this layer. The values of $\delta^{13}C$ and TOC in both cores PS51/154 (–25.6 ‰ and 0.79 %) and PS51/159 (–25.8 ‰ and 0.99 %) remained rather constant despite the periods of peak MAR (Fig S5). After the early Holocene (9.6 kyr BP), the $\delta^{13}C$ value increased, accompanied by a drop in sedimentation rate in both cores, indicating a decrease in terrestrial input resulting from fast marine transgression (Bauch et al., 2001; Mueller-Lupp et al., 2000; Bauch et al., 1999).

4.3 Lipid and lignin phenol records in cores PS51/154 and PS51/159

The P_{aq} index in core PS51/154 dropped to 0.29 between 17.0 and 16.0 kyr BP (Fig 2b), remained stable afterward, started to increase after 12.6 kyr BP, and reached its highest value of 0.42 at 10.8 kyr BP. In core PS51/159, the P_{aq} remained high (0.38) before the early Holocene and decreased afterward (Fig 2b).

In the record from core PS51/154, the Sd/Sl ratio was high (0.88) before 16.2 kyr BP (Fig 2c). The Sd/Sl ratio remained stable in both cores before 10 kyr BP, of 0.61 in PS51/154 and 0.67 in PS51/159. In core PS51/159, the Sd/Sl increased since 8.8 kyr BP and reached a stable high value of 0.84 after 6.0 kyr BP. The S/V ratio in core PS51/154 was low (0.64) before 16.0 kyr BP; the ratio increased afterward, peaked at 11.5 kyr BP with a ratio of 0.82, and decreased subsequently (Fig 3). The core PS51/159 record exhibited the same trend. The S/V ratio reached its highest of 0.94 at 11.9 kyr BP, decreased afterward, and reached a stable low value of 0.70 after 9.5 kyr BP (Fig 3). The C/V ratio remained constant (~0.51) in both records, except for one drop at the depth of the slump layer to 0.30 at 15.4 kyr BP in core PS51/154 (Fig 3).

https://doi.org/10.5194/cp-2024-60
Preprint. Discussion started: 18 September 2024

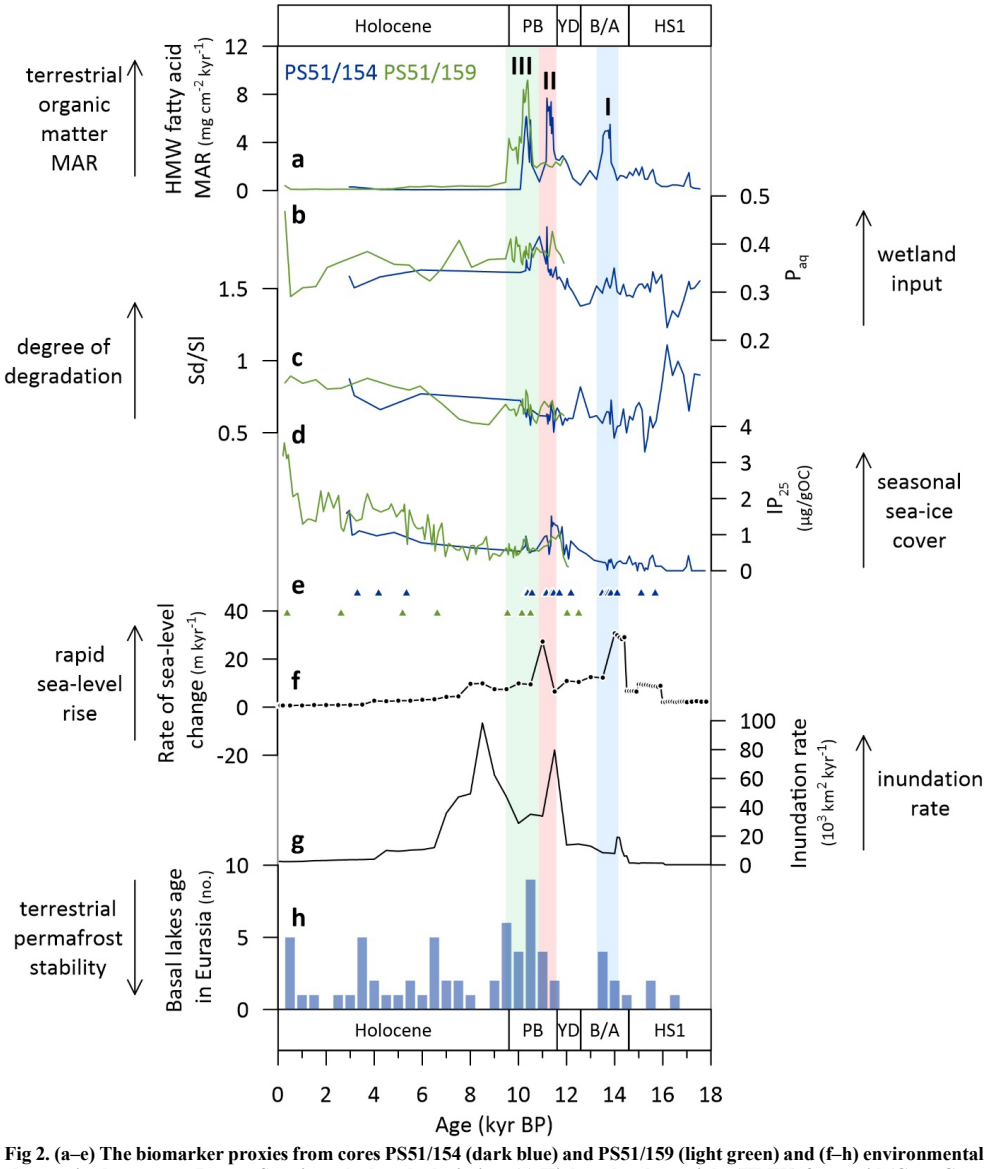

Fig 2. (a–e) The biomarker proxies from cores PS51/154 (dark blue) and PS51/159 (light green) and (f–h) environmental changes in the western Laptev Sea since the last deglaciation. (a) High molecular weight (HMW) fatty acid ($C_{26:0}$, $C_{28:0}$, $C_{30:0}$) mass accumulation rate (MAR) of cores PS51/154 and PS51/159 (this study), the MAR peaks are labeled with numbers. (b) P_{aq} values of cores PS51/154 and PS51/159 (this study). (c) Syringic acid/syringaldehyde ratio (Sd/Sl) of cores PS51/154 and PS51/159 (this study). (d) IP25 contents of cores PS51/154 and PS51/159 (Hörner et al., 2016). (e) Age-depth model controlling points from radiocarbon dating measurements of cores PS51/154 and PS51/159. (f) Rate of sea-level rise in the western Laptev Sea (Klemann et al., 2015). (g) Area of land inundation per kyr in the western Laptev Sea, calculated from the sea-level reconstruction from Klemann et al. (2015) and the bathymetric data from the international bathymetric chart of the Arctic Ocean (IBCAO) (Jakobsson et al., 2012). (h) Counts of newly developed thermokarst lakes, categorized by the basal ages of the reported thermokarst lakes (number within 500-yr bins) in Siberia (Brosius et al., 2021). The names of different paleoclimate periods are indicated by acronyms (HS1: Heinrich Stadial 1, B/A: Bølling-Allerød, YD: Younger Dryas, PB: Preboreal).

https://doi.org/10.5194/cp-2024-60
Preprint. Discussion started: 18 September 2024

Climate of the Past Discussions
Open Access
EGU

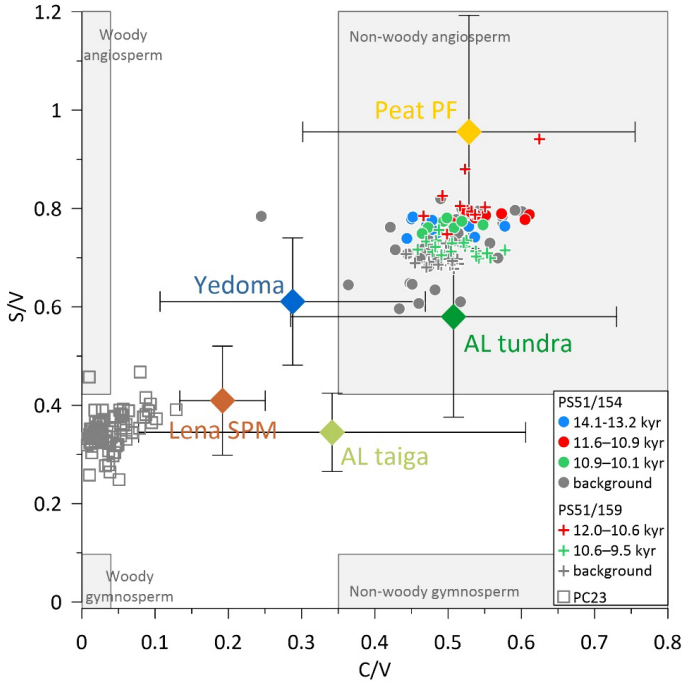

Fig 3. Vegetation source parameters derived from ratios of syringyl/vanillyl phenols (S/V) and cinnamyl/vanillyl phenols (C/V) of core records in the Laptev Sea and terrestrial records from Siberia. The core records include cores PS51/154 (dots, this study), PS51/159 (crosses, this study), and PC23 (Tesi et al., 2016b). For data from PS51/154 and PS51/159, symbol colors mark data from different organic matter MAR peaks: blue: MAR peak I period (from 14.1 to 13.2 kyr BP in core PS51/154); red: MAR peak II in core PS51/154 (from 11.6 to 10.9 kyr BP) and core bottom in core PS51/159 (from 12 to 10.6 kyr BP); green: MAR peak III (from 10.9 to 10.1 kyr BP in core PS51/154 and 10.6 to 9.5 kyr BP in core PS51/159). Diamond data points indicate Siberian terrestrial records, including Holocene peat permafrost collected from the Lena Delta (peat PF) (Winterfeld et al., 2015), suspended particulate matter from the Lena Delta (Lena SPM) (Winterfeld et al., 2015), Yedoma (Tesi et al., 2014), active layer from the tundra region (AL tundra) (Tesi et al., 2014), and active layer from the taiga region (AL taiga) (Tesi et al., 2014).

5 Discussion

5.1 Temporal changes of terrOM characteristics in the western Laptev Sea since the last deglaciation

The record from core PS51/154 before 16 kyr BP suggests that land-to-ocean terrOM transport was low, which could have resulted from permanent sea ice cover (Hörner et al., 2016) (Fig 2e) and the low terrestrial supply due to cold and dry hinterland condition (Andreev et al., 2003). Specifically, high $\delta^{13}C$ and low OC-normalized terrestrial biomarker contents suggest limited terrestrial organic matter input from land (Fig S5). The high Sd/Sl during this period indicates either enhanced degradation of the small amount of terrOM reaching the core site due to longer transport times from land to the shelf caused by sea ice blockage or, alternatively, the terrOM originated from an already degraded pool (Fig 2c).

Three distinct peaks of HMW fatty acid MAR were recorded in core PS51/154, occurring from 14.1 to 13.2 kyr BP (MAR peak I), from 11.6 to 10.9 kyr BP (MAR peak II), and from 10.9 to 10.1 kyr BP (MAR peak III) (Fig 2a). Core PS51/159 recorded one HMW fatty acid MAR peak, from 10.6 to 9.5 kyr BP (MAR peak III) (Fig 2a). The absence of MAR peaks before 10.6 kyr in core PS51/159 may be because the water depth at this location was too shallow, and the main sediment depocenter of the Laptev Sea was located further north at that time (Stein and

https://doi.org/10.5194/cp-2024-60
Preprint. Discussion started: 18 September 2024

Fahl, 2000; Bauch et al., 2001). The lack of MAR peak II could also be due to the lack of available chronology tie points in core PS51/159 during this period (Fig 2e).

Our records suggest that different mechanisms of terrOM mobilization led to varying terrOM characteristics. During the period of MAR peak I, rapid sea-level rise resulted in enhanced coastal erosion on the steep coast near the shelf break (Fig 4a). The intruding warm Atlantic seawater inhibited sea ice formation, further aggravating coastal erosion (Taldenkova et al., 2010; Hörner et al., 2016) (Fig 2a, d, f, Fig 4a). As observed in modern environments, coastal areas with high cliffs experience accelerated erosion when rapid sea-level rise causes waves to reach higher steep cliffs (Limber et al., 2018; Shadrick et al., 2022). The relatively cold and dry Siberian inland hindered wetland development (Fig 2h) (Hubberten et al., 2004; Brosius et al., 2021). The combination of enhanced coastal erosion and limited wetland sources is reflected in low P_{aq} and low S/V ratios during MAR peak I compared to the later MAR peak periods (Fig 4a, Fig 2b).

During the periods of MAR peak II and MAR peak III, increasing temperature and humidity in the Siberian hinterland facilitated contemporary wetland development as well as thermokarst slump formation, which exposed deep old peatland (Schuur et al., 2015; Hubberten et al., 2004; Yu et al., 2010) (Fig 2h). The Laptev Sea shelf was rapidly inundated due to its flat topography, and the inundation rate remained high even after the sea-level rise slowed down (Mueller-Lupp et al., 2000; Bauch et al., 2001; Klemann et al., 2015) (Fig 2g, Fig 4b, c). In coastal areas with gentle slopes, rapid sea-level rise results in accelerated marine transgression and inundates terrestrial permafrost. Seawater also increases the temperature of the inundated permafrost and facilitates thawing (Overduin et al., 2016). The peak P_{aq} values during this period indicate that terrestrial wetland deposits, either developed contemporarily or exposed from deep permafrost, were transported by river or/and widely flooded and mobilized (Fig 2b). The elevated wetland input during MAR peak II was also reflected by an increased soft angiosperm tissue contribution, originating from grass-like material abundant in Holocene peats and Holocene permafrost (Winterfeld et al., 2015) (Fig 3). The S/V ratio decreased during MAR peak III, indicating an elevated contribution of gymnosperm plants, likely reflecting the northward expansion of the conifer tree line due to rising temperature and humidity during this period (Wild et al., 2022; Hubberten et al., 2004) (Fig 2b, Fig 3). Our records highlight that changes in terrOM reflect varying inland permafrost stability and marine transgression scenarios. An additional source of brassicasterol, typically ascribed to marine diatoms, during the period of MAR peak II in core PS51/154 was attributed to increased river runoff during this period (Hörner et al., 2016). This additional river runoff was likely not originating from the Lena River, as the lignin phenol assemblages in core PS51/154 differed significantly from that of the nearby sediment core records (PC23) (Tesi et al., 2016b) and Lena River suspended particulate matter (Lena SPM) (Winterfeld et al., 2015) (Fig 3). Instead, the riverine terrOM deposited in the western Laptev Sea likely originated from the Olenyok or Khatanga Rivers rather than the Lena River (Fig 4b). This is supported by modern observations that most freshwater and suspended sediment discharged from the Lena River are transported eastward to the eastern Laptev Sea (Dmitrenko et al., 1999; Guay et al., 2001), and the mineral assemblages in the western Laptev Sea surface sediment sediments resemble those from the Khatanga River rather than the Lena River (Dethleff et al., 2000).

Overall, the S/V and C/V ratios in cores PS51/154 and PS51/159 are higher than those in the Lena SPM (Fig 3) (Winterfeld et al., 2015). The low S/V and C/V ratios in the Lena SPM suggest a significant contribution of woody gymnosperm tissues transported from boreal forests in the southern part of the Lena River catchment (Tesi et al., 2016b; Wild et al., 2022). In contrast, the higher S/V and C/V ratios in PS51/154 and PS51/159 indicate that the vegetation source of the western Laptev Sea primarily originated from higher latitudes, reflecting a regional signal.

https://doi.org/10.5194/cp-2024-60
Preprint. Discussion started: 18 September 2024

Climate of the Past Discussions
Open Access
EGU

This is further supported by the less degraded lignin phenol signals (lower Sd/Sl) in PS51/154 and PS51/159 compared to those in the Lena SPM, which could be due to either a shorter transport distance or a better-preserved organic matter that was freeze-locked in permafrost (Wild et al., 2022).

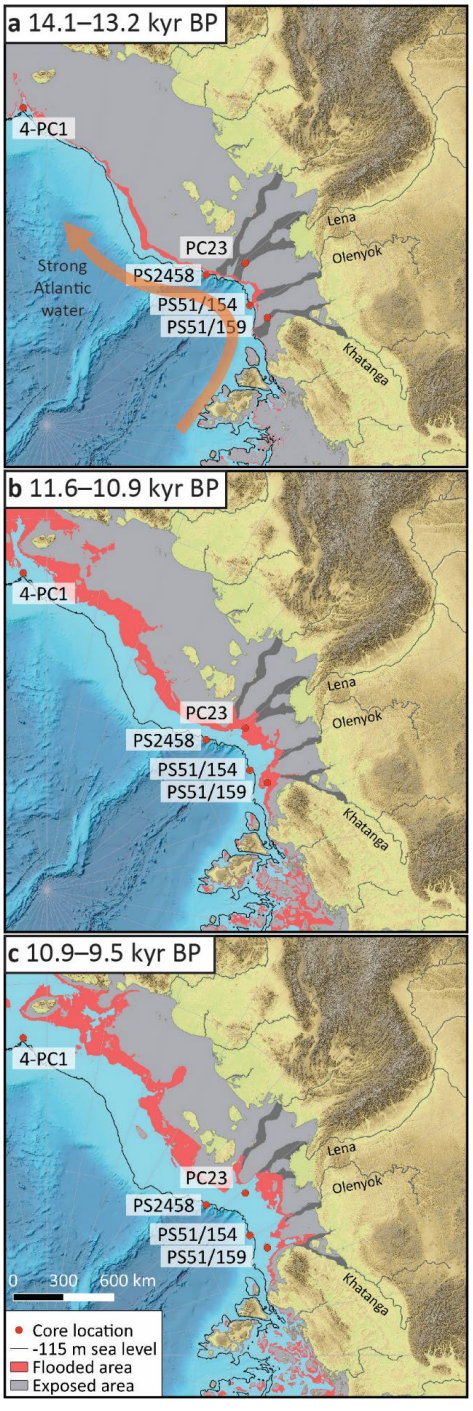

https://doi.org/10.5194/cp-2024-60
Preprint. Discussion started: 18 September 2024

Climate of the Past Discussions
Open Access
EGU

Fig 4. Flooded shelf area during the periods of high HMW fatty acid MAR recorded in cores PS51/154 and PS51/159. (a) MAR peak I, from 14.1 to 13.2 kyr BP. (b) MAR peak II, from 11.6 to 10.9 kyr BP. (c) MAR peak III, from 10.9 to 9.5 kyr BP. The grey area shows the exposed continental shelf. The red areas show the flooded area during the periods. The flooded and exposed areas are calculated using the modern bathymetry map from IBCAO (Jakobsson et al., 2012). The river data are from Lehner and Grill (2013). The dark grey areas denote the paleo river channel (Kleiber and Niessen, 2000). The thick black line denotes the contour of −115 m sea level, which approximates the sea level at 18 kyr BP. Red dots are the core locations in the Laptev Sea, including cores 4-PC1 (Martens et al., 2019), PC23 (Tesi et al., 2016b), PS2458 (Spielhagen et al., 2005), PS51/154 (this study), and PS51/159 (this study). The orange arrow indicates the period that the Laptev Sea shelf experienced a strong impact from Atlantic water (Taldenkova et al., 2010).

5.2 Environmental change affecting rapid organic matter transport to the ocean on pan-Arctic and regional scales

In order to evaluate whether the described terrOM MAR peaks reflected pan-Arctic scale climate dynamics, we compared our HMW fatty acid MAR results with other terrOM MAR records from the Arctic marginal seas. Studies have used different biomarkers to trace terrestrial inputs. Branched Glycerol Dialyl Glycerol Tetraethers (brGDGTs) are found in membrane lipids from soil bacteria. Campesterol and β-sitosterol are biosynthesized in vascular plants and thus reflect terrestrial signals, in contrast to dinosterol and brassicasterol, which are found abundant in marine plankton (Bianchi and Canuel, 2011). Data were collected from sites in the Beaufort Sea (ARA04C/37) (Wu et al., 2020), the Chukchi Sea (4-PC1) (Martens et al., 2019), the Laptev Sea (PC23) (Tesi et al., 2016b), the northern Svalbard continental margin (HH11-09) (Nogarotto et al., 2023), and the Fram Strait (PS2837-5 and MSM05/5-712-2) (Birgel and Hass, 2004; Aagaard-Sørensen et al., 2014; Müller and Stein, 2014; Zamelczyk et al., 2014). Further we included one terrOM MAR record from the high latitude northern hemisphere, Bering Sea (SO202-18-3/6), in our comparison (Meyer et al., 2019) (Fig 1, Fig 5). Records from the Chukchi and Bering Sea supplement the North American Arctic records. Before the Bering Strait opened at around 11 kyr BP (Jakobsson et al., 2017), the coastlines of the Beaufort Sea and the Chukchi Sea were connected, allowing the potential westward transport of terrOM from North America. Therefore, we consider the record before 11 kyr BP from the Chukchi Sea (4-PC1) as a representation of terrOM signal from the North American Arctic.

TerrOM MAR largely depends on changes in sedimentation rate, which can vary significantly between age models. Using age models with dense chronological control points is crucial. To ensure confidence in the timing of terrOM MAR peaks, we selected records with multiple chronological tie-points both below and above the identified terrOM MAR peaks (Fig 5d, e, f, h) or multiple records from the same region to provide a more comprehensive regional pattern (Fig 5i–j, k–m).

Age-depth models for these records were recalibrated against the Marine20 calibration curve (Heaton et al., 2020) or a combination of Intcal20 (Reimer et al., 2020) and Marine20 curves, depending on the original studies to achieve congruent age control across all records. Reservoir ages were taken from the original publications. We further calculated the age uncertainty of each terrOM MAR peak by including ±1-sigma uncertainty from the age models. The possible age ranges of these terrOM MAR peaks are shown in Fig 5. The only exception is the record SO202-18-3/6; as this was calibrated based on laminated sediments and ash layers, we adopted the age model published by Kuehn et al. (2014).

https://doi.org/10.5194/cp-2024-60
Preprint. Discussion started: 18 September 2024

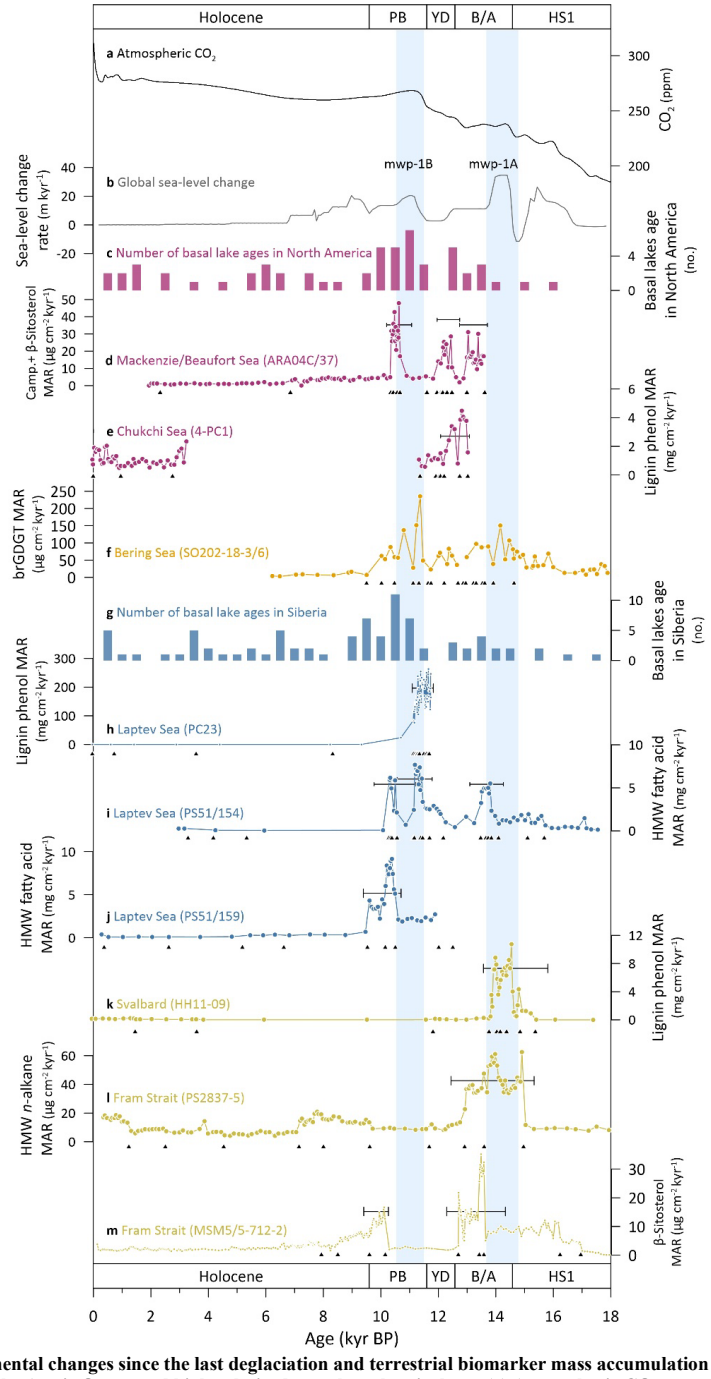

Fig 5. Environmental changes since the last deglaciation and terrestrial biomarker mass accumulation rates (MARs) of core records in the Arctic Ocean and higher-latitude northern hemisphere. (a) Atmospheric CO_2 concentration (Köhler et al., 2017). (b) Rate of global sea-level change (Lambeck et al., 2014). (c) Compilation of basal ages of thermokarst lakes (number within 500-yr bins) in North America (Brosius et al., 2021). (d) Campestreol+β-sitosterol MAR from core ARA04C/37, Beaufort Sea (Wu et al., 2020). (e) Lignin phenol MAR from core 4-PC1, Chukchi Sea (Martens et al., 2019). (f) brGDGT MAR from cores SO202-18-3/6, Bering Sea (Meyer et al., 2019). (g) Compilation of basal ages of thermokarst lakes (number within 500-yr bins) in Siberia (Brosius et al., 2021). (h) Lignin phenol MAR from core PC23, Laptev Sea (Tesi et al., 2016b). (i) HMW fatty acid MAR from core PS51/154, Laptev Sea (this study). (j) HMW fatty

https://doi.org/10.5194/cp-2024-60
Preprint. Discussion started: 18 September 2024

acid MAR from core PS51/159, Laptev Sea (this study). (k) Lignin phenol MAR from core HH11-09, northern Svalbard continental margin (Nogarotto et al., 2023). (l) HMW *n*-alkane MAR from core PS2837-5, Fram Strait (Birgel and Hass, 2004). (m) β-sitosterol MAR from core MSM05/5-712-2, Fram Strait (Müller and Stein, 2014; Aagaard-Sørensen et al., 2014; Zamelczyk et al., 2014). The blue bars highlight the period of rapid sea-level rise. The black intervals under each MAR peak indicate the age uncertainty range of the MAR peaks, calculated by the ±1-sigma age models. Meltwater pulses are denoted as mwp-1A and mwp-1B. The names of different paleoclimate periods are indicated by acronyms (HS1: Heinrich Stadial 1, B/A: Bølling-Allerød, YD: Younger Dryas, PB: Preboreal).

5.2.1 Pan-Arctic factor: sea-level rise

The rapid global sea-level rise during meltwater pulse 1A (mwp-1A) was an important process in terrOM mobilization across the pan-Arctic region. TerrOM MAR peaks during this period are observed widely in records from the Eurasian Arctic and the Bering Sea (Fig 5b, f, h–m) (Lambeck et al., 2014; Nogarotto et al., 2023; Birgel and Hass, 2004; Meyer et al., 2019). Inland temperatures in both North America and Siberia remained low during this time (Fig 5c, g). These concurrent terrOM MAR peaks suggest that rapid sea-level rise was the primary cause for pan-Arctic permafrost mobilization, possibly contributing to the rapid increase in atmospheric CO2 concentration (Marcott et al., 2014; Winterfeld et al., 2018). The lack of radiocarbon tie points below the peak makes it difficult to determine whether the late starting time of MAR peak in mwp-1A in core MSM05/5-712-2 from Fram Strait compared to other regional records may in fact be due to age model uncertainty or was a real feature.

During mwp-1B, terrOM MAR also increased in records from the Bering Sea and the Laptev Sea (Fig 5f, h, i). However, this peak was absent in records from North America and Svalbard/Fram Strait (Fig 5d, e, k, l). One of the possible reasons could be the lack of radiocarbon age controls in these cores during this period. Also, the amplitude of sea-level rise and even the existence of mwp-1B remain debated (Lambeck et al., 2014). The lack of widespread terrOM MAR during mwp-1B suggests that this event did not affect the pan-Arctic region as extensively as mwp-1A did. Still, records from SO202-18-3/6, PC23, and PS51/154 collected adjacent to areas that remained largely unglaciated during the LGM and were covered by extensive permafrost deposits show terrOM MAR peaks (Meyer et al., 2019; Tesi et al., 2016b), and we attribute this to a combination of rapid widespread inland warming and rapid sea-level rise during this period.

5.2.2 Regional factor: inland warming, sea ice loss, and freshwater pulses

Outside the periods of mwp-1A and mwp-1B (indicated by blue bars in Fig 5), several regional terrOM MAR peaks were observed in the Arctic marginal seas. These peaks were likely driven by regional inland warming. Warming facilitates permafrost thawing and thermokarst lake development (Schuur et al., 2015). Lake basal ages indicate the time of lake formation. A higher count of thermokarst lake formation in a certain period thus implies intense inland warming (Brosius et al., 2021). In the North American Arctic, terrOM MAR peaks appeared during the interval between mwp-1A and mwp-1B (Fig 5d, e). Inland warming in North American began at approximately 13.5 kyr BP, while the Eurasian Arctic remained cold (Brosius et al., 2021). This regional temperature discrepancy possibly explains the exclusive terrOM MAR peaks observed in the North American Arctic during the interval between mwp-1A and mwp-1B (Fig 5c, g) (apart from the Younger Dryas terrOM MAR peak in ARA04C/37, which is exclusively attributed to a fresh water flooding event; see the discussion below). TerrOM MAR peaks also appeared during the early Holocene across the North American Arctic, Siberian Arctic, and Fram Strait records (Fig 5d, e, h–j, m). During the early Holocene, enhanced warming in both North American and Siberian hinterlands led to elevated terrOM mobilization in both regions (Fig 5c, g). These terrOM MAR peaks occurred during periods

https://doi.org/10.5194/cp-2024-60
Preprint. Discussion started: 18 September 2024


Climate of the Past Discussions

of little sea-level variation, indicating that intensified inland warming could destabilize permafrost and result in regional terrOM mobilization even in the absence of rapid sea-level rise.

Notably, the observed terrOM MAR peaks in the Arctic marginal seas coincided with regionally reduced seasonal sea ice cover, as indicated by reduced IP_{25} (Wu et al., 2020; Hörner et al., 2016; Müller et al., 2009). IP_{25} refers to an alkane that is produced by sea ice associated diatoms. The existence of IP_{25} indicates the appearance of seasonal sea ice, while the lack of IP_{25} implies either the lack of seasonal sea ice or permanent sea ice coverage in the area (Belt and Müller, 2013). Studies have shown that accelerated coastal erosion can be mitigated by the presence of land-fast sea ice, which prevents thermal denudation by sea water, direct wave erosion, and saltwater intrusion into permafrost coasts (Rachold et al., 2000; Overduin et al., 2016; Irrgang et al., 2022; Nielsen et al., 2020). Modern observations have associated elevated coastal erosion rates in the Laptev Sea with reduced winter sea ice cover (Nielsen et al., 2020). Modeling studies also indicate a positive correlation between inland permafrost stability and winter sea ice extent under modern conditions (Vandenberghe et al., 2012). The MAR peak III in core PS51/154 and PS51/159 reflected that even without rapid sea-level rise, the mobilized material triggered by inland warming was more easily transported to marine basins because of the lack of sea-ice protection on the coast (Fig 2a, d). A similar relation was shown in the core from the Beaufort Sea (ARA04C/37) as the two terrestrial biomarker MAR peaks registered in the core both happened during an ice-free period (Wu et al., 2020). The Holocene record of core PS51/159 shows the opposite condition. The seasonal sea-ice cover started to increase since 7 kyr BP (Hörner et al., 2016). Even though several warming periods in Siberia were recorded since then, no terrestrial biomarker MAR peak was recorded in core PS51/159 (Fig 2a, e, h). The growing sea ice might play a role in protecting the warming land from being eroded and keeping the terrestrial material from being transported into the Laptev Sea shelf.

Freshwater floods triggered by ice-dammed lake breakings could be another regional factor in terrOM mobilization. These flooding events can be recorded by the decreasing stable oxygen isotope ratio ($\delta^{18}O$) in planktic foraminiferas (Spielhagen et al., 2005; Keigwin et al., 2018). In the North American Arctic record (ARA04C/37), the terrOM MAR peak occurring during the Younger Dryas was linked to a well-described meltwater flood event through the Mackenzie River, based on the drop of both $\delta^{18}O$ value in planktic foraminiferas and TOC (Wu et al., 2020; Klotsko et al., 2019; Keigwin et al., 2018) (Fig 5d). However, freshwater events were less likely to be the cause for terrOM MAR in the western Laptev Sea. While freshwater flooding events were recorded in an ice-dammed lake upstream of the Lena River (14.9 ± 2.0 kyr BP) and in a sediment record from the Laptev Sea (PS2458, at 12.7 ky BP) (Spielhagen et al., 2005; Margold et al., 2018), the timing of these events did not correspond with any of the terrOM MAR peaks in cores PS51/154 and PS51/159. This temporal mismatch suggests that Siberian freshwater pulses had little impact on the increase in terrestrial biomarker MAR in the western Laptev Sea.

6 Summary and Conclusions

This study explores temporal changes in the composition and rate of terrOM mobilization to the western Laptev Sea, as indicated by lipid and lignin phenol records. Three rapid terrigenous organic matter supply events were identified from 14.1 to 13.2, from 11.6 to 10.9, and from 10.9 to 9.5 kyr BP. Each peak showed different compositional characteristics, suggesting distinct terrOM sources derived from different mechanisms. The first terrOM MAR peak was likely driven by enhanced coastal erosion, while the latter two peaks were associated with

https://doi.org/10.5194/cp-2024-60
Preprint. Discussion started: 18 September 2024

inland warming and rapid shelf inundation. The source shift was characterized by increased wetland input, as evidenced by both P_{aq} and S/V ratios. Comparing our findings with records from across the pan-Arctic and northern hemisphere high latitude indicates that the enhanced terrOM mobilization during mwp-1A period was primarily driven by enhanced coastal erosion resulting from rapid global sea-level rise. However, terrOM MAR peaks did not always align with periods of rapid sea-level rise, suggesting that other regional factors, such as inland warming, lack of sea-ice protection, and freshwater floods, also played significant roles.

Overall, the study highlights that the topography of the western Laptev Sea shelf strongly influenced erosion scenarios linked to sea-level rise, leading to different terrOM sources mobilized from land to ocean. Our results suggest that while rapid sea-level rise contributed to elevated terrOM mobilization on a pan-Arctic scale, regional factors such as inland warming, freshwater floods, and sea ice cover decrease were responsible for regional terrOM mobilization.

Author contributions

GM designed the study; TWL, JH, HG, JW and AN performed the measurements; TWL, TT, JH, HG, FA, and GM analysed the data; FA and JW verified the age models; TWL wrote the manuscript draft with the support from TT and GM; all the coauthors reviewed and edited the manuscript.

Competing interests

The authors declare that they have no conflict of interest.

Acknowledgment

This study was supported by the German-Italian partnership project between Alfred Wegener Institute and CNR-ISP on Chronologies for Polar Paleoclimate Archives (PAIGE), funded by the Helmholtz Association. FA was supported through the Helmholtz association (VH-NG 1501). We thank the captain, the chief scientist, the crew, and the scientific party of the Polarstern Expedition ARK-XIV/1b (PS51 Transdrift-V) for providing the studied material. We thank Kirsten Fahl and Rüdiger Stein for offering coring information. We thank the MICADAS radiocarbon laboratory group members at Alfred Wegener Institute, namely Elizabeth Bonk, Torben Gentz, and Lea Philips. We appreciate help from Arnaud Nicolas in core subsampling. Katarzyna Zamelczyk and Steffen Aagaard Sørensen are acknowledged for dry bulk density data of core MSM05/5-712-2. ChatGPT (version GPT-4) was used in this manuscript to edit grammar and improve sentence fluency.

References

Aagaard-Sørensen, S., Husum, K., Werner, K., Spielhagen, R. F., Hald, M., and Marchitto, T. M.: A Late Glacial–Early Holocene multiproxy record from the eastern Fram Strait, Polar North Atlantic, Marine Geology, 355, 15-26, 10.1016/j.margeo.2014.05.009, 2014.

Alves, E. Q., Wong, W., Hefter, J., Grotheer, H., Tesi, T., Gentz, T., Zonneveld, K., and Mollenhauer, G.: Deglacial export of pre-aged terrigenous carbon to the Bay of Biscay, Climate of the Past Discussions, 2023, 1-21, https://doi.org/10.5194/cp-2023-7, 2023.

https://doi.org/10.5194/cp-2024-60
Preprint. Discussion started: 18 September 2024

Andreev, A. A., Tarasov, P. E., Siegert, C., Ebel, T., Klimanov, V. A., Melles, M., Bobrov, A. A., Dereviagin, A. Y., Lubinski, D. J., and Hubberten, H. W.: Late Pleistocene and Holocene vegetation and climate on the northern Taymyr Peninsula, Arctic Russia, Boreas, 32, 484-505, 2003.

Are, F., Grigoriev, M. N., Hubberten, H.-W., Rachold, V., Razumov, S., and Schneider, W.: Comparative shoreface evolution along the Laptev Sea coast, Polarforschung, 135-150, 2002.

Bauch, H. A., Kassens, H., Erlenkeuser, H., Grootes, P. M., and Thiede, J.: Depositional environment of the Laptev Sea (Arctic Siberia) during the Holocene, Boreas, 28, 194-204, 1999.

Bauch, H. A., Mueller-Lupp, T., Taldenkova, E., Spielhagen, R. F., Kassens, H., Grootes, P. M., Thiede, J., Heinemeier, J., and Petryashov, V.: Chronology of the Holocene transgression at the North Siberian margin, Global Planetary Change, 31, 125-139, 2001.

Belt, S. T. and Müller, J.: The Arctic sea ice biomarker IP25: a review of current understanding, recommendations for future research and applications in palaeo sea ice reconstructions, Quaternary Science Reviews, 79, 9-25, 2013.

Bianchi, T. S. and Canuel, E. A.: Chemical biomarkers in aquatic ecosystems, in: Chemical Biomarkers in Aquatic Ecosystems, Princeton University Press, 2011.

Birgel, D. and Hass, H.: Oceanic and atmospheric variations during the last deglaciation in the Fram Strait (Arctic Ocean): a coupled high-resolution organic-geochemical and sedimentological study, Quaternary Science Reviews, 23, 29-47, 10.1016/j.quascirev.2003.10.001, 2004.

Bronk Ramsey, C.: Bayesian Analysis of Radiocarbon Dates, Radiocarbon, 51, 337-360, 10.1017/s0033822200033865, 2009.

Brosius, L. S., Anthony, K. M. W., Treat, C. C., Lenz, J., Jones, M. C., Bret-Harte, M. S., and Grosse, G.: Spatiotemporal patterns of northern lake formation since the Last Glacial Maximum, Quaternary Science Reviews, 253, 10.1016/j.quascirev.2020.106773, 2021.

Clark, P. U., Shakun, J. D., Baker, P. A., Bartlein, P. J., Brewer, S., Brook, E., Carlson, A. E., Cheng, H., Kaufman, D. S., Liu, Z., Marchitto, T. M., Mix, A. C., Morrill, C., Otto-Bliesner, B. L., Pahnke, K., Russell, J. M., Whitlock, C., Adkins, J. F., Blois, J. L., Clark, J., Colman, S. M., Curry, W. B., Flower, B. P., He, F., Johnson, T. C., Lynch-Stieglitz, J., Markgraf, V., McManus, J., Mitrovica, J. X., Moreno, P. I., and Williams, J. W.: Global climate evolution during the last deglaciation, Proceedings of the National Academy of Sciences of the United States of America, 109, E1134-1142, 10.1073/pnas.1116619109, 2012.

Dethleff, D.: Entrainment and export of Laptev Sea ice sediments, Siberian Arctic, Journal of Geophysical Research: Oceans, 110, 10.1029/2004jc002740, 2005.

Dethleff, D., Rachold, V., Tintelnot, M., and Antonow, M.: Sea-ice transport of riverine particles from the Laptev Sea to Fram Strait based on clay mineral studies, International Journal of Earth Sciences, 89, 496-502, 2000.

Detlef, H., O'Regan, M., Stranne, C., Jensen, M. M., Glasius, M., Cronin, T. M., Jakobsson, M., and Pearce, C.: Seasonal sea-ice in the Arctic's last ice area during the Early Holocene, Communications Earth & Environment, 4, 10.1038/s43247-023-00720-w, 2023.

Dmitrenko, I., Golovin, P., Gribanov, V., and Kassens, H.: Oceanographic causes for transarctic ice transport of river discharge, in: Land-Ocean Systems in the Siberian Arctic, edited by: Kassens, H., Bauch, H. A., Dmitrenko, I. A., Eicken, H., Hubberten, H.-W., Melles, M., Thiede, J., and Timokhov, L. A., Springer Berlin, Heidelberg, 73-92, 1999.

Dobinski, W.: Permafrost, Earth-Science Reviews, 108, 158-169, 10.1016/j.earscirev.2011.06.007, 2011.

https://doi.org/10.5194/cp-2024-60
Preprint. Discussion started: 18 September 2024

Dyke, A. S., Moore, A., and Robertson, L.: Deglaciation of North America [dataset], https://doi.org/10.4095/214399, 2003.

Fahl, K. and Stein, R.: Modern seasonal variability and deglacial/Holocene change of central Arctic Ocean sea-ice cover: New insights from biomarker proxy records, Earth and Planetary Science Letters, 351-352, 123-133, 10.1016/j.epsl.2012.07.009, 2012.

Ficken, K. J., Li, B., Swain, D., and Eglinton, G.: An n-alkane proxy for the sedimentary input of submerged/floating freshwater aquatic macrophytes, Organic Geochemistry, 31, 745-749, 2000.

Goñi, M. A. and Hedges, J. I.: Lignin dimers: Structures, distribution, and potential geochemical applications, Geochimica et Cosmochimica Acta, 56, 4025-4043, 1992.

Goñi, M. A. and Montgomery, S.: Alkaline CuO oxidation with a microwave digestion system: Lignin analyses of geochemical samples, Analytical Chemistry, 72, 3116-3121, 2000.

Grotheer, H., Robert, A. M., Greenwood, P. F., and Grice, K.: Stability and hydrogenation of polycyclic aromatic hydrocarbons during hydropyrolysis (HyPy) – Relevance for high maturity organic matter, Organic Geochemistry, 86, 45-54, 10.1016/j.orggeochem.2015.06.007, 2015.

Guay, C. K., Falkner, K. K., Muench, R. D., Mensch, M., Frank, M., and Bayer, R.: Wind-driven transport pathways for Eurasian Arctic river discharge, Journal of Geophysical Research, 106, 11469-11480, 2001.

Günther, F., Overduin, P. P., Yakshina, I. A., Opel, T., Baranskaya, A. V., and Grigoriev, M. N.: Observing Muostakh disappear: permafrost thaw subsidence and erosion of a ground-ice-rich island in response to arctic summer warming and sea ice reduction, The Cryosphere, 9, 151-178, 2015.

Haddad, R., Newell, S., Martens, C., and Fallon, R.: Early diagenesis of lignin-associated phenolics in the salt marsh grass Spartina alterniflora, Geochimica et Cosmochimica Acta, 56, 3751-3764, 1992.

Heaton, T. J., Köhler, P., Butzin, M., Bard, E., Reimer, R. W., Austin, W. E. N., Bronk Ramsey, C., Grootes, P. M., Hughen, K. A., Kromer, B., Reimer, P. J., Adkins, J., Burke, A., Cook, M. S., Olsen, J., and Skinner, L. C.: Marine20—The Marine Radiocarbon Age Calibration Curve (0–55,000 cal BP), Radiocarbon, 62, 779-820, 10.1017/rdc.2020.68, 2020.

Hedges, J. I. and Mann, D. C.: The characterization of plant tissues by their lignin oxidation products, Geochimica et Cosmochimica Acta, 43, 1803-1807, 1979.

Hedges, J. I., Blanchette, R. A., Weliky, K., and Devol, A. H.: Effects of fungal degradation on the CuO oxidation products of lignin: a controlled laboratory study, Geochimica et Cosmochimica Acta, 52, 2717-2726, 1988.

Holmes, R., Shiklomanov, A. I., Suslova, A., Tretiakov, M., McClelland, J., Scott, L., Spencer, R., and Tank, S.: River discharge, United States. National Oceanic and Atmospheric Administration. Office of Oceanic and Atmospheric Research ;Global Ocean Monitoring and Observing (GOMO) Program;, https://doi.org/10.25923/zevf-ar65, 2021.

Hörner, T., Stein, R., Fahl, K., and Birgel, D.: Post-glacial variability of sea ice cover, river run-off and biological production in the western Laptev Sea (Arctic Ocean)–A high-resolution biomarker study, Quaternary Science Reviews, 143, 133-149, 2016.

Hubberten, H. W., Andreev, A., Astakhov, V. I., Demidov, I., Dowdeswell, J. A., Henriksen, M., Hjort, C., Houmark-Nielsen, M., Jakobsson, M., Kuzmina, S., Larsen, E., Lunkka, J. P., Lysa, A., Mangerud, J., Möller, P., Saarnisto, M., Schirrmeister, L., Sher, A. V., Siegert, C., Siegert, M. J., and Svendsen, J. I.: The periglacial climate and environment in northern Eurasia during the Last Glaciation, Quaternary Science Reviews, 23, 1333-1357, 10.1016/j.quascirev.2003.12.012, 2004.

https://doi.org/10.5194/cp-2024-60
Preprint. Discussion started: 18 September 2024

Hugelius, G., Strauss, J., Zubrzycki, S., Harden, J. W., Schuur, E. A. G., Ping, C. L., Schirrmeister, L., Grosse, G., Michaelson, G. J., Koven, C. D., O'Donnell, J. A., Elberling, B., Mishra, U., Camill, P., Yu, Z., Palmtag, J., and Kuhry, P.: Estimated stocks of circumpolar permafrost carbon with quantified uncertainty ranges and identified data gaps, Biogeosciences, 11, 6573-6593, 10.5194/bg-11-6573-2014, 2014.

Hughes, A. L., Gyllencreutz, R., Lohne, Ø. S., Mangerud, J., and Svendsen, J. I.: The last Eurasian ice sheets–a chronological database and time-slice reconstruction, DATED-1, Boreas, 45, 1-45, 2016.

Irrgang, A. M., Bendixen, M., Farquharson, L. M., Baranskaya, A. V., Erikson, L. H., Gibbs, A. E., Ogorodov, S. A., Overduin, P. P., Lantuit, H., Grigoriev, M. N., and Jones, B. M.: Drivers, dynamics and impacts of changing Arctic coasts, Nature Reviews Earth & Environment, 3, 39-54, 10.1038/s43017-021-00232-1, 2022.

Jakobsson, M., Mayer, L., Coakley, B., Dowdeswell, J. A., Forbes, S., Fridman, B., Hodnesdal, H., Noormets, R., Pedersen, R., and Rebesco, M.: The international bathymetric chart of the Arctic Ocean (IBCAO) version 3.0, Geophysical Research Letters, 39, 2012.

Jakobsson, M., Pearce, C., Cronin, T. M., Backman, J., Anderson, L. G., Barrientos, N., Björk, G., Coxall, H., de Boer, A., Mayer, L. A., Mörth, C.-M., Nilsson, J., Rattray, J. E., Stranne, C., Semiletov, I., and O'Regan, M.: Post-glacial flooding of the Bering Land Bridge dated to 11 cal ka BP based on new geophysical and sediment records, Climate of the Past, 13, 991-1005, 10.5194/cp-13-991-2017, 2017.

Kassens, H.: Station list and links to master tracks in different resolutions of POLARSTERN cruise ARK-XIV/1b, Tiksi - Tromsø, 1998-07-28 - 1998-08-28, PANGAEA [dataset], https://doi.org/10.1594/PANGAEA.858867, 2016.

Keigwin, L. D., Klotsko, S., Zhao, N., Reilly, B., Giosan, L., and Driscoll, N. W.: Deglacial floods in the Beaufort Sea preceded Younger Dryas cooling, Nature Geoscience, 11, 599-604, 10.1038/s41561-018-0169-6, 2018.

Keskitalo, K., Tesi, T., Bröder, L., Andersson, A., Pearce, C., Sköld, M., Semiletov, I. P., Dudarev, O. V., and Gustafsson, Ö.: Sources and characteristics of terrestrial carbon in Holocene-scale sediments of the East Siberian Sea, Climate of the Past, 13, 1213-1226, 10.5194/cp-13-1213-2017, 2017.

Kleiber, H. P. and Niessen, F.: Variations of continental discharge pattern in space and time: implications from the Laptev Sea continental margin, Arctic Siberia, International Journal of Earth Sciences, 89, 605-616, 10.1007/s005310000130, 2000.

Klemann, V., Heim, B., Bauch, H. A., Wetterich, S., and Opel, T.: Sea-level evolution of the Laptev Sea and the East Siberian Sea since the last glacial maximum, Arktos, 1, 10.1007/s41063-015-0004-x, 2015.

Klotsko, S., Driscoll, N., and Keigwin, L.: Multiple meltwater discharge and ice rafting events recorded in the deglacial sediments along the Beaufort Margin, Arctic Ocean, Quaternary Science Reviews, 203, 185-208, 10.1016/j.quascirev.2018.11.014, 2019.

Köhler, P., Nehrbass-Ahles, C., Schmitt, J., Stocker, T. F., and Fischer, H.: A 156 kyr smoothed history of the atmospheric greenhouse gases CO2, CH4, and N2O and their radiative forcing, Earth System Science Data, 9, 363-387, 10.5194/essd-9-363-2017, 2017.

Kuehn, H., Lembke-Jene, L., Gersonde, R., Esper, O., Lamy, F., Arz, H., Kuhn, G., and Tiedemann, R.: Laminated sediments in the Bering Sea reveal atmospheric teleconnections to Greenland climate on millennial to decadal timescales during the last deglaciation, Climate of the Past, 10, 2215-2236, 10.5194/cp-10-2215-2014, 2014.

Kuptsov, V. and Lisitsin, A.: Radiocarbon of Quaternary along shore and bottom deposits of the Lena and the Laptev Sea sediments, Marine Chemistry, 53, 301-311, 1996.

https://doi.org/10.5194/cp-2024-60
Preprint. Discussion started: 18 September 2024

Lambeck, K., Rouby, H., Purcell, A., Sun, Y., and Sambridge, M.: Sea level and global ice volumes from the Last Glacial Maximum to the Holocene, Proceedings of the National Academy of Sciences of the United States of America, 111, 15296-15303, 10.1073/pnas.1411762111, 2014.

Lantuit, H., Atkinson, D., Paul Overduin, P., Grigoriev, M., Rachold, V., Grosse, G., and Hubberten, H.-W.: Coastal erosion dynamics on the permafrost-dominated Bykovsky Peninsula, north Siberia, 1951–2006, Polar Research, 30, 10.3402/polar.v30i0.7341, 2011.

Lara, M. J., Lin, D. H., Andresen, C., Lougheed, V. L., and Tweedie, C. E.: Nutrient release from permafrost thaw enhances CH4 emissions from arctic tundra wetlands, Journal of Geophysical Research: Biogeosciences, 124, 1560-1573, 10.1029/2018jg004641, 2019.

Laurent, M., Fuchs, M., Herbst, T., Runge, A., Liebner, S., and Treat, C.: Relationships between greenhouse gas production and landscape position during short-term permafrost thaw under anaerobic conditions in the Lena Delta., Biogeosciences, 20, 2049-2064, 10.5194/bg-2022-122, 2023.

Lehner, B. and Grill, G.: Global river hydrography and network routing: baseline data and new approaches to study the world's large river systems, Hydrological Processes, 27, 2171-2186, 2013.

Limber, P. W., Barnard, P. L., Vitousek, S., and Erikson, L. H.: A Model Ensemble for Projecting Multidecadal Coastal Cliff Retreat During the 21st Century, Journal of Geophysical Research: Earth Surface, 123, 1566-1589, 10.1029/2017jf004401, 2018.

Liu, S., Wang, P., Huang, Q., Yu, J., Pozdniakov, S. P., and Kazak, E. S.: Seasonal and spatial variations in riverine DOC exports in permafrost-dominated Arctic river basins, Journal of Hydrology, 612, 10.1016/j.jhydrol.2022.128060, 2022.

Marcott, S. A., Bauska, T. K., Buizert, C., Steig, E. J., Rosen, J. L., Cuffey, K. M., Fudge, T. J., Severinghaus, J. P., Ahn, J., Kalk, M. L., McConnell, J. R., Sowers, T., Taylor, K. C., White, J. W., and Brook, E. J.: Centennial-scale changes in the global carbon cycle during the last deglaciation, Nature, 514, 616-619, 10.1038/nature13799, 2014.

Margold, M., Jansen, J. D., Codilean, A. T., Preusser, F., Gurinov, A. L., Fujioka, T., and Fink, D.: Repeated megafloods from glacial Lake Vitim, Siberia, to the Arctic Ocean over the past 60,000 years, Quaternary Science Reviews, 187, 41-61, 10.1016/j.quascirev.2018.03.005, 2018.

Martens, J., Wild, B., Muschitiello, F., O'Regan, M., Jakobsson, M., Semiletov, I., Dudarev, O. V., and Gustafsson, Ö.: Remobilization of dormant carbon from Siberian-Arctic permafrost during three past warming events, Science Advances, 6, eabb6546, 2020.

Martens, J., Wild, B., Pearce, C., Tesi, T., Andersson, A., Broder, L., O'Regan, M., Jakobsson, M., Skold, M., Gemery, L., Cronin, T. M., Semiletov, I., Dudarev, O. V., and Gustafsson, O.: Remobilization of Old Permafrost Carbon to Chukchi Sea Sediments During the End of the Last Deglaciation, Global Biogeochemical Cycles, 33, 2-14, 10.1029/2018GB005969, 2019.

McClelland, J. W., Holmes, R. M., Peterson, B. J., Raymond, P. A., Striegl, R. G., Zhulidov, A. V., Zimov, S. A., Zimov, N., Tank, S. E., Spencer, R. G. M., Staples, R., Gurtovaya, T. Y., and Griffin, C. G.: Particulate organic carbon and nitrogen export from major Arctic rivers, Global Biogeochemical Cycles, 30, 629-643, 10.1002/2015gb005351, 2016.

Meyer, V. D., Hefter, J., Köhler, P., Tiedemann, R., Gersonde, R., Wacker, L., and Mollenhauer, G.: Permafrost-carbon mobilization in Beringia caused by deglacial meltwater runoff, sea-level rise and warming, Environmental Research Letters, 14, 10.1088/1748-9326/ab2653, 2019.

https://doi.org/10.5194/cp-2024-60
Preprint. Discussion started: 18 September 2024

675 Miller, G. H., Alley, R. B., Brigham-Grette, J., Fitzpatrick, J. J., Polyak, L., Serreze, M. C., and White, J. W. C.: Arctic amplification: can the past constrain the future?, Quaternary Science Reviews, 29, 1779-1790, 10.1016/j.quascirev.2010.02.008, 2010.

Mollenhauer, G., Grotheer, H., Gentz, T., Bonk, E., and Hefter, J.: Standard operation procedures and performance of the MICADAS radiocarbon laboratory at Alfred Wegener Institute (AWI), Germany, Nuclear Instruments and 680 Methods in Physics Research Section B: Beam Interactions with Materials and Atoms, 496, 45-51, 10.1016/j.nimb.2021.03.016, 2021.

Mueller-Lupp, T., Bauch, H. A., Erlenkeuser, H., Hefter, J., Kassens, H., and Thiede, J.: Changes in the deposition of terrestrial organic matter on the Laptev Sea shelf during the Holocene: evidence from stable carbon isotopes, International Journal of Earth Sciences, 89, 563-568, 10.1007/s005310000128, 2000.

685 Müller, J. and Stein, R.: High-resolution record of late glacial and deglacial sea ice changes in Fram Strait corroborates ice–ocean interactions during abrupt climate shifts, Earth and Planetary Science Letters, 403, 446-455, 10.1016/j.epsl.2014.07.016, 2014.

Müller, J., Massé, G., Stein, R., and Belt, S. T.: Variability of sea-ice conditions in the Fram Strait over the past 30,000 years, Nature Geoscience, 2, 772-776, 10.1038/ngeo665, 2009.

690 Nielsen, D. M., Dobrynin, M., Baehr, J., Razumov, S., and Grigoriev, M.: Coastal Erosion Variability at the Southern Laptev Sea Linked to Winter Sea Ice and the Arctic Oscillation, Geophysical Research Letters, 47, 10.1029/2019gl086876, 2020.

Nogarotto, A., Noormets, R., Chauhan, T., Mollenhauer, G., Hefter, J., Grotheer, H., Belt, S., Colleoni, F., Muschitiello, F., Capotondi, L., Pellegrini, C., and Tesi, T.: Coastal permafrost was massively eroded during the 695 Bølling-Allerød warm period, Communications Earth & Environment, 4, 350, https://doi.org/10.1038/s43247-023-01013-y, 2023.

Overduin, P. P., Wetterich, S., Günther, F., Grigoriev, M. N., Grosse, G., Schirrmeister, L., Hubberten, H.-W., and Makarov, A.: Coastal dynamics and submarine permafrost in shallow water of the central Laptev Sea, East Siberia, The Cryosphere, 10, 1449-1462, 10.5194/tc-10-1449-2016, 2016.

700 Rachold, V., Grigoriev, M. N., Are, F. E., Solomon, S., Reimnitz, E., Kassens, H., and Antonow, M.: Coastal erosion vs riverine sediment discharge in the Arctic Shelf seas, International Journal of Earth Sciences, 89, 450-460, 10.1007/s005310000113, 2000.

Rantanen, M., Karpechko, A. Y., Lipponen, A., Nordling, K., Hyvärinen, O., Ruosteenoja, K., Vihma, T., and Laaksonen, A.: The Arctic has warmed nearly four times faster than the globe since 1979, Communications Earth 705 & Environment, 3, 10.1038/s43247-022-00498-3, 2022.

Reimer, P. J., Austin, W. E. N., Bard, E., Bayliss, A., Blackwell, P. G., Bronk Ramsey, C., Butzin, M., Cheng, H., Edwards, R. L., Friedrich, M., Grootes, P. M., Guilderson, T. P., Hajdas, I., Heaton, T. J., Hogg, A. G., Hughen, K. A., Kromer, B., Manning, S. W., Muscheler, R., Palmer, J. G., Pearson, C., van der Plicht, J., Reimer, R. W., Richards, D. A., Scott, E. M., Southon, J. R., Turney, C. S. M., Wacker, L., Adolphi, F., Büntgen, U., Capano, M., 710 Fahrni, S. M., Fogtmann-Schulz, A., Friedrich, R., Köhler, P., Kudsk, S., Miyake, F., Olsen, J., Reinig, F., Sakamoto, M., Sookdeo, A., and Talamo, S.: The IntCal20 Northern Hemisphere Radiocarbon Age Calibration Curve (0–55 cal kBP), Radiocarbon, 62, 725-757, 10.1017/rdc.2020.41, 2020.

Rigor, I. and Colony, R.: Sea-ice production and transport of pollutants in the Laptev Sea, 1979–1993, Science of the Total Environment, 202, 89-110, 1997.

https://doi.org/10.5194/cp-2024-60
Preprint. Discussion started: 18 September 2024

715 Rudenko, O., Tarasov, P. E., Bauch, H. A., and Taldenkova, E.: A Holocene palynological record from the northeastern Laptev Sea and its implications for palaeoenvironmental research, Quaternary International, 348, 82-92, 10.1016/j.quaint.2014.04.032, 2014.

Schuur, E. A., Bockheim, J., Canadell, J. G., Euskirchen, E., Field, C. B., Goryachkin, S. V., Hagemann, S., Kuhry, P., Lafleur, P. M., and Lee, H.: Vulnerability of permafrost carbon to climate change: Implications for the global 720 carbon cycle, BioScience, 58, 701-714, 2008.

Schuur, E. A., McGuire, A. D., Schadel, C., Grosse, G., Harden, J. W., Hayes, D. J., Hugelius, G., Koven, C. D., Kuhry, P., Lawrence, D. M., Natali, S. M., Olefeldt, D., Romanovsky, V. E., Schaefer, K., Turetsky, M. R., Treat, C. C., and Vonk, J. E.: Climate change and the permafrost carbon feedback, Nature, 520, 171-179, 10.1038/nature14338, 2015.

725 Shadrick, J. R., Rood, D. H., Hurst, M. D., Piggott, M. D., Hebditch, B. G., Seal, A. J., and Wilcken, K. M.: Sea-level rise will likely accelerate rock coast cliff retreat rates, Nature Communications, 13, 7005, 10.1038/s41467-022-34386-3, 2022.

Spielhagen, R., Erlenkeuser, H., and Siegert, C.: History of freshwater runoff across the Laptev Sea (Arctic) during the last deglaciation, Global and Planetary Change, 48, 187-207, 10.1016/j.gloplacha.2004.12.013, 2005.

730 Stein, R. and Fahl, K.: Holocene accumulation of organic carbon at the Laptev Sea continental margin (Arctic Ocean): sources, pathways, and sinks, Geo-Marine Letters, 20, 27-36, 2000.

Stein, R. and Macdonald, R. W., Stein, R., and MacDonald, R. W. (Eds.): The organic carbon cycle in the Arctic Ocean, Springer Berlin, Heidelberg, https://doi.org/10.1007/978-3-642-18912-8, 2004.

Strauss, J., Schirrmeister, L., Mangelsdorf, K., Eichhorn, L., Wetterich, S., and Herzschuh, U.: Organic-matter 735 quality of deep permafrost carbon – a study from Arctic Siberia, Biogeosciences, 12, 2227-2245, 10.5194/bg-12-2227-2015, 2015.

Strauss, J., Schirrmeister, L., Grosse, G., Fortier, D., Hugelius, G., Knoblauch, C., Romanovsky, V., Schädel, C., Schneider von Deimling, T., Schuur, E. A. G., Shmelev, D., Ulrich, M., and Veremeeva, A.: Deep Yedoma permafrost: A synthesis of depositional characteristics and carbon vulnerability, Earth-Science Reviews, 172, 75-740 86, 10.1016/j.earscirev.2017.07.007, 2017.

Strauss, J., Laboor, S., Fedorov, A. N., Fortier, D., Froese, D. G., Fuchs, M., Grosse, G., Günther, F., Harden, J. W., Hugelius, G., Kanevskiy, M. Z., Kholodov, A. L., Kunitsky, V. V., Kraev, G., Lapointe-Elmrabti, L., Lozhkin, A. V., Rivkina, E., Robinson, J., Schirrmeister, L., Shmelev, D., Shur, Y., Siegert, C., Spektor, V., Ulrich, M., Vartanyan, S. L., Veremeeva, A., Walter Anthony, K. M., and Zimov, S. A.: Database of Ice-Rich Yedoma 745 Permafrost (IRYP) [dataset], https://doi.org/10.1594/PANGAEA.861733, 2016.

Strauss, J., Laboor, S., Schirrmeister, L., Fedorov, A. N., Fortier, D., Froese, D., Fuchs, M., Günther, F., Grigoriev, M., Harden, J., Hugelius, G., Jongejans, L. L., Kanevskiy, M., Kholodov, A., Kunitsky, V., Kraev, G., Lozhkin, A., Rivkina, E., Shur, Y., Siegert, C., Spektor, V., Streletskaya, I., Ulrich, M., Vartanyan, S., Veremeeva, A., Anthony, K. W., Wetterich, S., Zimov, N., and Grosse, G.: Circum-Arctic Map of the Yedoma Permafrost Domain, 750 Frontiers in Earth Science, 9, 10.3389/feart.2021.758360, 2021.

Strauss, J., Laboor, S., Schirrmeister, L., Fedorov, A. N., Fortier, D., Froese, D. G., Fuchs, M., Günther, F., Grigoriev, M. N., Harden, J. W., Hugelius, G., Jongejans, L. L., Kanevskiy, M. Z., Kholodov, A. L., Kunitsky, V., Kraev, G., Lozhkin, A. V., Rivkina, E., Shur, Y., Siegert, C., Spektor, V., Streletskaya, I., Ulrich, M., Vartanyan, S. L., Veremeeva, A., Walter Anthony, K. M., Wetterich, S., Zimov, N. S., and Grosse, G.: Database of Ice-Rich 755 Yedoma Permafrost Version 2 (IRYP v2), PANGAEA [dataset], 10.1594/PANGAEA.940078, 2022.

https://doi.org/10.5194/cp-2024-60
Preprint. Discussion started: 18 September 2024

Taldenkova, E., Bauch, H. A., Gottschalk, J., Nikolaev, S., Rostovtseva, Y., Pogodina, I., Ovsepyan, Y., and Kandiano, E.: History of ice-rafting and water mass evolution at the northern Siberian continental margin (Laptev Sea) during Late Glacial and Holocene times, Quaternary Science Reviews, 29, 3919-3935, 2010.

Tesi, T., Puig, P., Palanques, A., and Goñi, M. A.: Lateral advection of organic matter in cascading-dominated submarine canyons, Progress in Oceanography, 84, 185-203, 10.1016/j.pocean.2009.10.004, 2010.

Tesi, T., Semiletov, I., Dudarev, O., Andersson, A., and Gustafsson, Ö.: Matrix association effects on hydrodynamic sorting and degradation of terrestrial organic matter during cross-shelf transport in the Laptev and East Siberian shelf seas, Journal of Geophysical Research: Biogeosciences, 121, 731-752, 10.1002/2015jg003067, 2016a.

Tesi, T., Semiletov, I., Hugelius, G., Dudarev, O., Kuhry, P., and Gustafsson, Ö.: Composition and fate of terrigenous organic matter along the Arctic land–ocean continuum in East Siberia: Insights from biomarkers and carbon isotopes, Geochimica et Cosmochimica Acta, 133, 235-256, 10.1016/j.gca.2014.02.045, 2014.

Tesi, T., Muschitiello, F., Smittenberg, R. H., Jakobsson, M., Vonk, J. E., Hill, P., Andersson, A., Kirchner, N., Noormets, R., Dudarev, O., Semiletov, I., and Gustafsson, O.: Massive remobilization of permafrost carbon during post-glacial warming, Nature Communications, 7, 13653, 10.1038/ncomms13653, 2016b.

van Everdingen, R. O., van Everdingen, R. O. (Ed.): Multi-language glossary of permafrost and related ground-ice terms, International Permafrost Association, Calgary, Alberta, Canada, 159 pp.2005.

Vandenberghe, J., Renssen, H., Roche, D. M., Goosse, H., Velichko, A. A., Gorbunov, A., and Levavasseur, G.: Eurasian permafrost instability constrained by reduced sea-ice cover, Quaternary Science Reviews, 34, 16-23, 10.1016/j.quascirev.2011.12.001, 2012.

Vonk, J. E. and Gustafsson, Ö.: Permafrost-carbon complexities, Nature Geoscience, 6, 675-676, 2013.

Wild, B., Shakhova, N., Dudarev, O., Ruban, A., Kosmach, D., Tumskoy, V., Tesi, T., Grimm, H., Nybom, I., Matsubara, F., Alexanderson, H., Jakobsson, M., Mazurov, A., Semiletov, I., and Gustafsson, O.: Organic matter composition and greenhouse gas production of thawing subsea permafrost in the Laptev Sea, Nature Communications, 13, 5057, 10.1038/s41467-022-32696-0, 2022.

Winterfeld, M., Goñi, M. A., Just, J., Hefter, J., and Mollenhauer, G.: Characterization of particulate organic matter in the Lena River delta and adjacent nearshore zone, NE Siberia – Part 2: Lignin-derived phenol compositions, Biogeosciences, 12, 2261-2283, 10.5194/bg-12-2261-2015, 2015.

Winterfeld, M., Mollenhauer, G., Dummann, W., Kohler, P., Lembke-Jene, L., Meyer, V. D., Hefter, J., McIntyre, C., Wacker, L., Kokfelt, U., and Tiedemann, R.: Deglacial mobilization of pre-aged terrestrial carbon from degrading permafrost, Nature Communications, 9, 3666, 10.1038/s41467-018-06080-w, 2018.

Wu, J., Stein, R., Fahl, K., Syring, N., Nam, S.-I., Hefter, J., Mollenhauer, G., and Geibert, W.: Deglacial to Holocene variability in surface water characteristics and major floods in the Beaufort Sea, Communications Earth & Environment, 1, 10.1038/s43247-020-00028-z, 2020.

Yu, Z., Loisel, J., Brosseau, D. P., Beilman, D. W., and Hunt, S. J.: Global peatland dynamics since the Last Glacial Maximum, Geophysical Research Letters, 37, 10.1029/2010gl043584, 2010.

Zamelczyk, K., Rasmussen, T. L., Husum, K., Godtliebsen, F., and Hald, M.: Surface water conditions and calcium carbonate preservation in the Fram Strait during marine isotope stage 2, 28.8–15.4 kyr, Paleoceanography, 29, 1-12, 2014.

https://doi.org/10.5194/cp-2024-60
Preprint. Discussion started: 18 September 2024

795 Zhang, T., Li, D., East, A. E., Walling, D. E., Lane, S., Overeem, I., Beylich, A. A., Koppes, M., and Lu, X.: Warming-driven erosion and sediment transport in cold regions, Nature Reviews Earth & Environment, 3, 832-851, 10.1038/s43017-022-00362-0, 2022.